

Cage-size control of guest vibration and thermal conductivity in $\text{Sr}_8\text{Ga}_{16}\text{Si}_{30-x}\text{Ge}_x$

K. Suekuni¹, M. A. Avila¹, K. Umeo^{1,2}, T. Takabatake^{1,3}

¹*Department of Quantum Matter, ADSM, ²Materials Science Center, N-BARD,*

³*Institute for Advanced Materials Research, Hiroshima University, Higashi-Hiroshima 739-8530, Japan*

(Dated: March 23, 2022)

We present a systematic study of thermal conductivity, specific heat, electrical resistivity, thermopower and x-ray diffraction measurements performed on single-crystalline samples of the pseudo-quaternary type-I clathrate system $\text{Sr}_8\text{Ga}_{16}\text{Si}_{30-x}\text{Ge}_x$, in the full range of $0 \leq x \leq 30$. All the samples show metallic behavior with n -type majority carriers. However, the thermal conductivity and specific heat strongly depend on x . Upon increasing x from 0 to 30, the lattice parameter increases by 3%, from 10.446 to 10.726 Å, and the localized vibrational energies of the Sr guest ions in the tetrakaidekahedron (dodecahedron) cages decrease from 59 (120) K to 35 (90) K. Furthermore, the lattice thermal conductivity at low temperatures is largely suppressed. In fact, a crystalline peak found at 15 K for $x = 0$ gradually decreases and disappears for $x \geq 20$, evolving into the anomalous glass-like behavior observed for $x = 30$. It is found that the increase of the free space for the Sr guest motion directly correlates with a continuous transition from on-center harmonic vibration to off-center anharmonic vibration, with consequent increase in the coupling strength between the guest's low-energy modes and the cage's acoustic phonon modes.

PACS numbers: 72.15.Jf, 72.20.Pa, 82.75.-z

I. INTRODUCTION

Semiconducting clathrate compounds are attracting considerable attention because of their potential for thermoelectric conversion applications.¹ The efficiency of a thermoelectric material at a given operation temperature T can be quantified by the dimensionless figure of merit $ZT = S^2T/\rho(\kappa_{el} + \kappa_L)$, where S , ρ , κ_{el} , κ_L , are the thermopower, electrical resistivity, electronic thermal conductivity and lattice thermal conductivity of the material, respectively. Intermetallic clathrates are compounds consisting of polyhedral cages (basically formed by Si, Ge and Sn through diamond-like bonding) that are normally filled with monovalent or divalent guest cations.^{2,3} Many of them follow the Zintl rule, where the cage atoms are partially substituted by acceptor atoms for charge compensation between guests and cages. In addition to the large $S(T)$ and small $\kappa_{el}(T)$ often observed in Zintl materials, the most pronounced feature of the clathrates is their very low lattice thermal conductivity κ_L (of order 1 W/m K at room temperature).^{4,5,6,7} Some of these compounds even show glasslike temperature-dependant thermal conductivity, although they crystallize in well-defined structures. Therefore, clathrates are good candidates to fulfill the phonon-glass electron-crystal (PGEC) concept,⁸ which is a guideline to search for high-performance thermoelectric materials with the very rare combination of simultaneously low thermal conductivity and electrical resistivity. The determination of which mechanisms are dominant in lowering $\kappa_L(T)$ in clathrates presents motivation from the performance improvement perspective, as well as from that of further understanding the physics behind atoms vibrating in unconventional crystalline lattices.

Among the several possible structures formed by these materials, the type-I clathrate structure adopted by the

$\text{A}_8\text{Ga}_{16}\text{Ge}_{30}$ group ($A = \text{Ba}, \text{Sr}$ and Eu) has shown particularly favorable thermoelectric properties.^{4,5,6,7} The unit cell of this bcc structure ($Pm\bar{3}n$, No. 223) consists of 46 cage atoms arranged in two dodecahedra and six tetrakaidekahedra, which incorporate two A atoms at the $2a$ site and six A atoms at the $6d$ site, respectively.^{2,3} Initial investigations of $\text{A}_8\text{Ga}_{16}\text{Ge}_{30}$ clearly indicated that the κ_L below room temperature was lowered in direct relation to the decrease of the guest atom's ionic radius (Ba^{+2} largest, Eu^{+2} smallest), whereas the lattice parameter of the three compounds remains relatively unchanged.⁶ This suggested that the general lowering in thermal conductivity is not so much related to the mass of the guest ions, but rather realized by the fact that they are loosely bound to an oversized cage, giving rise to an anomalous vibration showing low-frequency, non-dispersive localized modes (rattling) which couple to the heat-carrying acoustic phonon modes of the rigid cage structure and scatter them efficiently.^{5,9,10,11,12}

In addition, $\kappa(T)$ for $\text{Ba}_8\text{Ga}_{16}\text{Ge}_{30}$ exhibited a large peak at 15 K, being characteristic of a crystal lattice.⁶ By contrast, $\kappa(T)$ for $\text{Sr}_8\text{Ga}_{16}\text{Ge}_{30}$ and $\text{Eu}_8\text{Ga}_{16}\text{Ge}_{30}$ showed all of the characteristics of a structural glass.^{4,5,6} Neutron diffraction measurements⁶ revealed that the Ba atom in the large cage is located essentially at the center of the cage ($6d$ site), whereas a substantial probability exists for the Sr atom to move off the site center about 0.3 Å, to one of four crystallographically equivalent positions ($24j$ or $24k$ sites), and Eu atoms move away even more, 0.4 Å from the $6d$ site, suggesting that off-center rattling may be necessary to produce glass-like thermal conductivity.^{13,14,15,16} At lower temperature, nuclear tunneling among the four sites^{17,18,19} may also play the role. The on-center vibrational freedom of the Ba ions can be adequately described assuming independent harmonic oscillators (Einstein model),^{6,13,20,21,22} but the

TABLE I: Starting (flux) composition, crystal composition, lattice parameter a , electrical resistivity ρ , thermopower S and carrier concentration n at room temperature of $\text{Sr}_8\text{Ga}_{16}\text{Si}_{30-x}\text{Ge}_x$

	starting composition	Sr	:	Ga	:	Si	:	Ge	a (Å)	ρ_{280K} (mΩ cm)	S_{280K} (μV/K)	n ($10^{20}/\text{cm}^3$)
$x=0$	8 : 38 : 30 : 0	8	:	13.6	:	32.4	:	0	10.446	0.26	-13	46
5	8 : 38 : 24 : 6	8	:	13.7	:	27.0	:	5.3	10.483	0.28	-26	40
20	8 : 38 : 15 : 15	8	:	15.7	:	10.0	:	20.3	10.638	0.68	-60	16
26	8 : 38 : 6 : 24	8	:	15.9	:	4.0	:	26.1	10.703	1.23	-133	10
30	8 : 38 : 0 : 30	8	:	15.9	:	0	:	30.1	10.726	1.85	-200	4

Sr and Eu vibration cannot be satisfactorily modeled this way, indicating that anharmonic vibration contributions gain significance in these cases.¹³ For $\text{Sr}_8\text{Ga}_{16}\text{Ge}_{30}$, the anomalous specific heat contribution of the Sr ions was successfully reproduced by using a soft-potential model.²¹ The appearance of a plateau in $\kappa(T)$ and a broadened maximum in C/T^3 were interpreted as resultant from the low-energy excitations associated with anharmonic, quasi-localized vibrations of the Sr ions in the cage.

As an added degree of complexity, later investigations on several Ba-based clathrates have shown a strong dependence of the thermal conductivity on the majority charge carrier type,^{20,23} such that compounds with n -type carriers show low-temperature crystalline peaks in $\kappa(T)$ while their p -type counterparts show significantly lower and glasslike $\kappa(T)$ in the same temperature interval.^{20,22,23,24,25} These results appear inconsistent with the idea of the guest ion vibration having the relevant role in producing the glass-like behavior. An alternate model^{20,24,26,27} based on phonon-scattering by charge carriers²⁸ was proposed instead, and the question of which factors are dominant at low temperatures remains a currently open debate.²²

Given this scenario, it seemed instructive to pursue an investigation of the guest vibrational behaviors and their effect on thermal conductivity from the opposite approach, by maintaining the guest atom and carrier type fixed, while varying the cage environment in a controlled and systematic manner. The compound $\text{Sr}_8\text{Ga}_{16-y}\text{Si}_{30+y}$ ($0 \leq y \leq 5$) has only been characterized structurally so far^{2,29,30} and was reported to adopt the same type-I clathrate structure as $\text{As}_8\text{Ga}_{16}\text{Ge}_{30}$. The lattice parameter is somewhat dependent on y due to the size difference between Ga and Si, but remains between 10.460 Å ($y = 0$) and 10.408 Å ($y = 5$), therefore about 3% smaller than that of $\text{Sr}_8\text{Ga}_{16}\text{Ge}_{30}$.² Furthermore, partial solid solutions of Si-Ge in a clathrate structure have already been realized in polycrystalline $\text{Ba}_8\text{Ga}_{16}\text{Si}_{30-x}\text{Ge}_x$.^{31,32} Based on all the aforementioned, the pseudo-quaternary system $\text{Sr}_8\text{Ga}_{16}\text{Si}_{30-x}\text{Ge}_x$ appears to offer a suitable opportunity for investigating the relationships between cage size, guest vibration and

thermal conductivity. Indeed, we will show that homogeneous single-crystalline samples within the full range $0 \leq x \leq 30$ can be achieved and, upon increase of x and expansion of the cage size, we find a continuous evolution from on-center harmonic vibration and crystal-like $\kappa_L(T)$, to off-center anharmonic vibration and glass-like $\kappa_L(T)$.

II. EXPERIMENTAL

Polyhedral single crystals of 1-5 mm in diam. were grown from a self-flux method using excess Ga. High purity elements were mixed in an atomic ratio of $\text{Sr}:\text{Ga}:\text{Si}:\text{Ge} = 8:38:(30-X):X$ ($X = 0, 6, 15, 24, 30$) in an argon filled glovebox. The mixture was sealed in an evacuated and carbonized quartz tube, soaked at 1180 °C for 2-3 h, cooled over 10 h to 1000 °C and then slowly cooled over 100 h to 800-700 °C. At this point the ampoules were quickly removed from the furnace and the remaining molten Ga flux was separated by centrifuging. The composition of the crystals was examined by electron probe microanalysis (EPMA) with a wave length dispersive JEOL JXA-8200 system. The results are shown in Table I. The compositions of Si and Ge in the crystals are somewhat different from the starting compositions, and Ga is deficient in the Si rich crystals. Hereafter, the Ge content in the crystal x is used to denote the $\text{Sr}_8\text{Ga}_{16}\text{Si}_{30-x}\text{Ge}_x$ samples.

The crystal structures were refined with powder x-ray diffraction (XRD). The spectra of all samples shown in Fig. 1 were indexed on the basis of the type-I clathrate structure. Since both the atomic size and bond length of Ge are larger than for Si, the lattice parameter linearly increases as x increases from 0 to 30 in the series of samples, such that there is a 3% difference between the end compounds (see inset). For $x = 20$ and 26, higher angle peaks like [530] and [611] are visibly broadened, possibly due to the disorder among Si, Ga and Ge atoms. Electrical resistivity, thermopower and Hall coefficient were measured in home-made systems by a standard DC four-probe method, differential method and DC technique, respectively in the temperature range from 4 to 300 K.

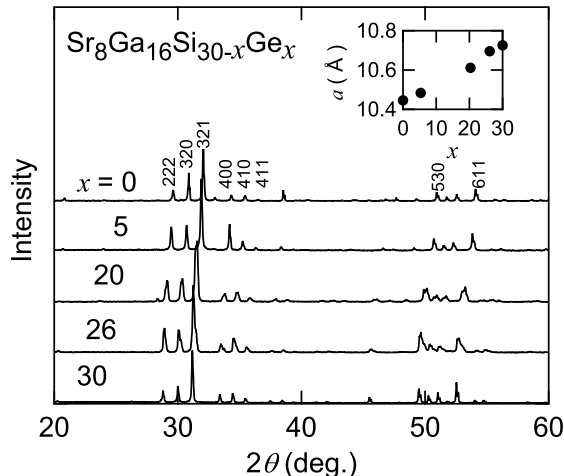


FIG. 1: Powder x-ray diffraction spectra (Cu $K\alpha$ radiation) for the $\text{Sr}_8\text{Ga}_{16}\text{Si}_{30-x}\text{Ge}_x$ specimens, and refined lattice parameters (inset).

Thermal conductivity experiments were performed using a steady-state method in a home-made cryostat. The data is reliable up to about 150 K, above which the effect of thermal losses by radiation and wire conduction require corrections. The specific heat from 0.3 to 300 K was measured using a Quantum Design PPMS with a thermal-relaxation method.

III. RESULTS AND DISCUSSION

The values of electrical resistivity (ρ), thermopower (S), and carrier concentration (n) at room temperature are listed in Table I. The latter was estimated from the Hall coefficient assuming one type of carriers. The decreasing trend in n with increasing x is consistent with the systematic increase of ρ ($T = 280$ K) from 0.26 to 1.85 m Ω cm. The temperature dependences of ρ and S are shown in Fig. 2. The monotonic decrease of $\rho(T)$ upon cooling is characteristic of heavily doped semiconductors or low carrier density metals. For all samples, S is negative and the absolute value increases monotonically with the increase of x . These variations of the transport properties can be attributed to a systematic decrease in n , from $46 \times 10^{20}/\text{cm}^3$ to $3.6 \times 10^{20}/\text{cm}^3$. This arises from the fact that Si-rich samples tend to be Ga deficient (see Table I and refs. 2,29,30) while Ge-rich samples follow the Zintl rule more strictly, and are therefore less electron-doped than Si-rich samples.

The specific heats are plotted as C/T^3 vs. T in Fig. 3. In this plotting style, the contribution of rattling ions appears as a broad peak over an electronic and Debye “background” from the stiff cage. Upon cooling, C/T^3 for all samples initially rises into the broad peak, followed by a local minimum, and finally rises again as $1/T^2$ due to

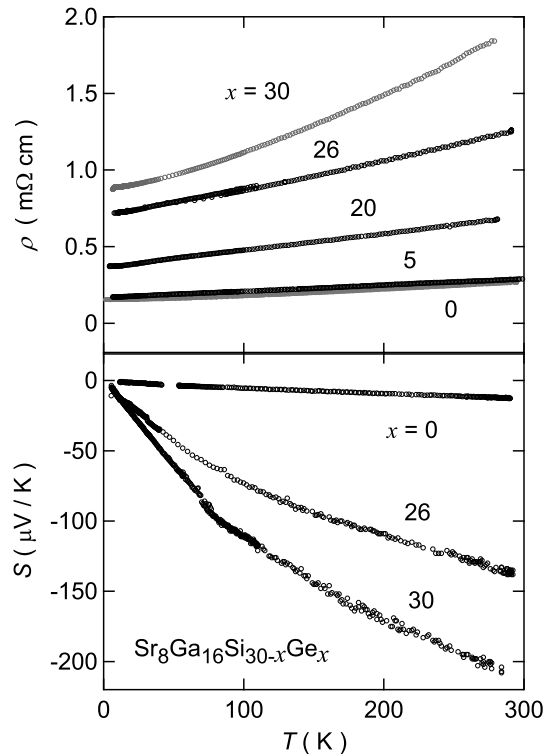


FIG. 2: Temperature dependence of electrical resistivity ρ and thermopower S for $\text{Sr}_8\text{Ga}_{16}\text{Si}_{30-x}\text{Ge}_x$.

the contribution from conduction electron and/or tunneling of guest ions. With increasing x , the peak height rises systematically and its temperature shifts from 10.5 K to 7 K. This is not related to n , whose contribution becomes vanishingly small at temperatures above 4 K. Rather, it is already a qualitative demonstration of how the rattling of the Sr ions increases in direct relation to the cage size. Further information about the Sr vibration characteristics can be obtained through a more careful analysis of the data as follows, using the same methodology we previously developed to analyze the data of C of $\text{Ba}_8\text{Ga}_{16}\text{Ge}_{30}$.²²

As a first approximation, the Sr atoms can be considered independent Einstein oscillators, and the framework composed of $(\text{Ga},\text{Si},\text{Ge})_{46}$ cages a stiff Debye solid. Following this approach, C of $\text{Sr}_8\text{Ga}_{16}\text{Si}_{30-x}\text{Ge}_x$ is treated as a sum of three terms: an electronic contribution C_{el} , a Debye contribution C_D , and an Einstein contribution C_E . As we described in detail in ref. 22, first the Sommerfeld coefficient γ and the Debye temperature θ_D should be evaluated independently and fixed, together with the pre-defined dimensionalities and numbers of Einstein oscillators, so that only two fitting parameters are left, which characterize the Sr guests vibrational energies. It should be recalled that the six $\text{Sr}_{(6d)}$ ions show a strongly anisotropic vibration with greater amplitude within the plane parallel to the larger cage’s two hexagons.⁵ Because

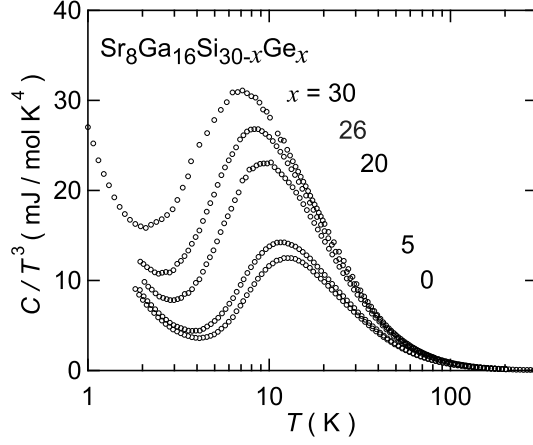


FIG. 3: Temperature dependence of specific heat C for $\text{Sr}_8\text{Ga}_{16}\text{Si}_{30-x}\text{Ge}_x$, presented as C/T^3 vs T .

the dimensionality plays a role in the Einstein model, at least two vibrational modes should be required to describe the $6d$ site alone: in-plane $\theta_{E(6d)}^{\parallel}$ and out-of-plane $\theta_{E(6d)}^{\perp}$, respectively.¹⁰ In addition, a third vibrational mode $\theta_{E(2a)}$ is required to account for the smaller, but still Einstein-type rattling of the two $\text{Sr}_{(2a)}$ which can be assumed isotropic.⁶ In our model, the dimensionalities and numbers of oscillators are predefined: $N_{E(2a)} = 3 \times 2$, $N_{E(6d)}^{\parallel} = 2 \times 6$, $N_{E(6d)}^{\perp} = 1 \times 6$. We impose the additional constraints $\theta_{E(6d)}^{\parallel} < \theta_{E(6d)}^{\perp}, \theta_{E(2a)}, \theta_{E(6d)}^{\parallel} = \theta_{EL}$ and $\theta_{E(6d)}^{\perp} = \theta_{E(2a)} = \theta_{EH}$, so the fitting parameters are only the lower and higher Einstein temperatures, θ_{EL} and θ_{EH} respectively.

From C/T vs. T^2 plots (not shown) the obtained values of γ are between 11 and 24 mJ/mol K², and the θ_D decreases from 370 K to 200 K on going from $x = 0$ to 30. However, as we discussed previously,²¹ when $\text{Sr}_{(6d)}$ anharmonic vibration becomes relevant it interferes with this evaluation even at the lowest temperatures. In fact, this last value of 200 K for θ_D of $\text{Sr}_8\text{Ga}_{16}\text{Ge}_{30}$ is an artifact, much smaller than 312 K estimated from atomic displacement parameters.²⁶ Thus, we use the value of 288 K obtained for $\text{Ba}_8\text{Ga}_{16}\text{Ge}_{30}$ as a better representation of the Ga-Ge cages' Debye temperature for $\text{Sr}_8\text{Ga}_{16}\text{Ge}_{30}$. For $x = 5, 20, 26$, θ_D is estimated by linear interpolation between the values for $x = 0$ and $x = 30$.

Fig. 4 shows the fits to the data of C/T^3 for $x = 0, 20$ and 30. For $x = 0$, an excellent fit is obtained with $\theta_{EL} = 59$ K and $\theta_{EH} = 120$ K, indicating that the assumption of independent, harmonic oscillators contained within the Einstein model applies very well for the Sr vibration in $\text{Sr}_8\text{Ga}_{16}\text{Si}_{30}$. By $x = 20$ it is clear that the fit with the Einstein model is no longer a good representation for the data, and at $x = 30$ the model has become completely inadequate to reproduce the behavior. This is a clear indication of the effects caused by increasingly

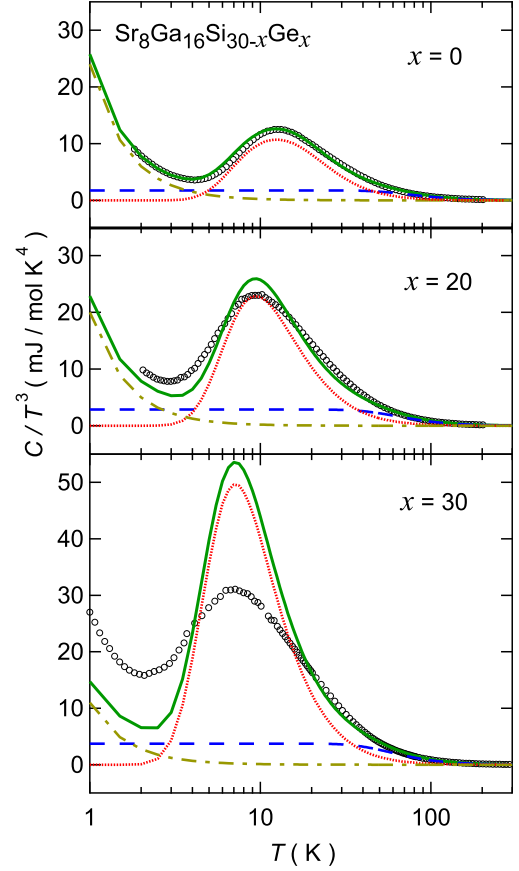


FIG. 4: (Color online) Einstein model fits (green solid lines) of the C/T^3 data (symbols). The dotted, dashed and dashed-dotted lines are the calculated C_E , C_D , and C_{el} , respectively (see text).

anharmonic vibration of the $\text{Sr}_{(6d)}$ guest ions, as their potential well broadens in direct proportion to the free space available for movement.¹⁰ In such a case, a soft potential model gives a good fit to $C(T)$.²¹ To our knowledge, however, there are no theoretical models available that can describe the $C(T)$ in this continuous transition from harmonic to anharmonic vibration observed in our sample series. For $x = 30$, the value of $\theta_{EL} = 35$ K determined mainly by the peak position is in good agreement with the result of 38 K observed by Raman scattering.¹² The Einstein temperatures θ_{EL} and θ_{EH} for all samples are listed in Table II.

Let us now see how all of these systematic changes affect the heat transport, which is our main purpose. The total thermal conductivity κ of $\text{Sr}_8\text{Ga}_{16}\text{Si}_{30-x}\text{Ge}_x$ is plotted as a function of temperature up to 150 K in Fig. 5. We can see two types of systematic evolutions in the data with increasing x : (i) κ at higher temperature decreases by a factor of 3, and (ii) a low temperature crystalline peak for $x = 0$ is gradually but strongly suppressed, resulting in glasslike behavior for $x = 30$. The

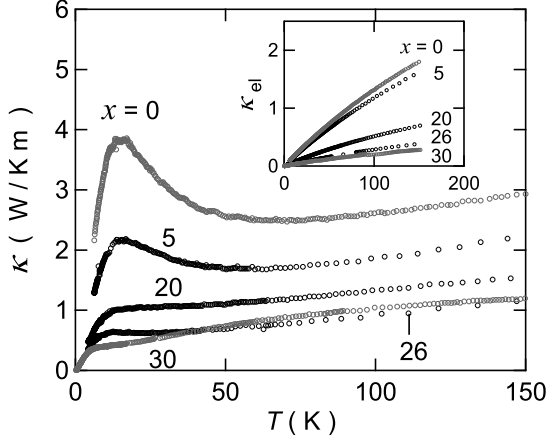


FIG. 5: Temperature dependence of total thermal conductivity κ . The inset shows the estimated electronic part κ_{el} .

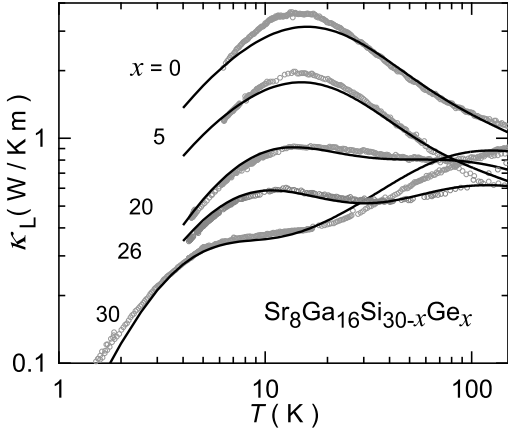


FIG. 6: Temperature dependence of lattice thermal conductivity κ_L . The solid lines are fits using the TRR model described in the text.

first effect can be directly attributed to the electronic contribution $\kappa_{el}(T)$, which is estimated from the electrical resistivity $\rho(T)$ using the Wiedemann-Franz law, $\kappa_{el}(T) = (\pi^2 k_B^2 / 3e^2) T / \rho(T)$. As shown in the inset of Fig. 5, $\kappa_{el}(T)$ have a simple, slightly sublinear behavior with slopes directly related to the carrier concentration, and therefore no relevant effect on the low temperature peak.

By subtracting $\kappa_{el}(T)$ from $\kappa(T)$, we can estimate the lattice contributions $\kappa_L(T)$, which are shown in Fig. 6. The values are now much closer at temperatures above 100 K, and an interesting feature reveals itself in this range: the heat conduction level of the pseudo-quaternary (intermediate) samples is lowered with respect to the ternary (end) samples. This is most likely the effect of extra phonon scattering on Ga/Si/Ge site disorder on the cage.

TABLE II: Parameters used for the solid line curves in Fig. 4 and Fig. 6.

Parameter	Unit	$x=0$	5	20	26	30
θ_{EL}	K	59	56	45.5	40.5	35
θ_{EH}	K	120	115	100	94	90
C_1	$10^{30}/(\text{m s}^2 \text{ K}^2)$	0.3	0.5	1.3	2.1	4.2
C_2	$10^{30}/(\text{m s}^2 \text{ K}^2)$	0.1	0.16	0.4	0.7	1.4
A/B	$10^5/(\text{m K})$	0.65	1.1	3.5	4	4.5
D	$1/(\text{m K}^4)$	1.5	3	2	3	1.5
θ_D	K	370	355	315	300	288

At lower temperatures, the plot shows a clearer picture of the peak suppression. We will analyze the data using the same approach described in detail in ref. 22. For lack of a single model capable of describing all sample behaviors in $C(T)$, we use the results of the Einstein model fittings despite their poor quality in Ge-rich samples. This is justifiable in our comparative analysis because $\kappa_L(T)$, given in the semiclassical theory by

$$\kappa_L = \frac{1}{3} \int_0^{\omega_D} d\omega [C_L(\omega, T) \nu l], \quad (1)$$

is not limited by the lattice specific heat $C_L(\omega, T)$, nor the average sound velocity ν , but rather by the very low phonon mean free path l , which is averaged over all major contributing scattering mechanisms. In the TRR model,⁷ l is written as

$$l = (l_{TS}^{-1} + l_{res}^{-1} + l_{Ray}^{-1})^{-1} + l_{min} \quad (2)$$

which includes three mechanisms: tunneling between localized guest sites, resonance scattering from guest ion rattling and Rayleigh scattering from impurities, imperfections and mass difference.

The best fits to the data are shown as solid lines in Fig. 6 and the parameter values are summarized in Table II. The most relevant results are the increase by one order of magnitude in both the resonant scattering level C_i and the TS scattering level as x increases. The latter can be expressed by the ratio $A/B = \tilde{n}(\hbar\nu)^2/k_B$, which in glasses is essentially a measure of subset density of tunneling states \tilde{n} that are able to strongly couple to the phonons and effectively scatter them.³³ For $x = 5, 20, 26$, Si disorder among Ga and Ge makes Rayleigh scattering level larger than that for $x = 0$ and 30.

Thus, the combined results of lattice $C_L(T)$ and $\kappa_L(T)$ can be clearly attributed to a systematic evolution of the $\text{Sr}_{(6d)}$ guests rattling level, with a decrease in characteristic energy and increase in anharmonicity, both arising from the fact that the lattice expansion increases the free

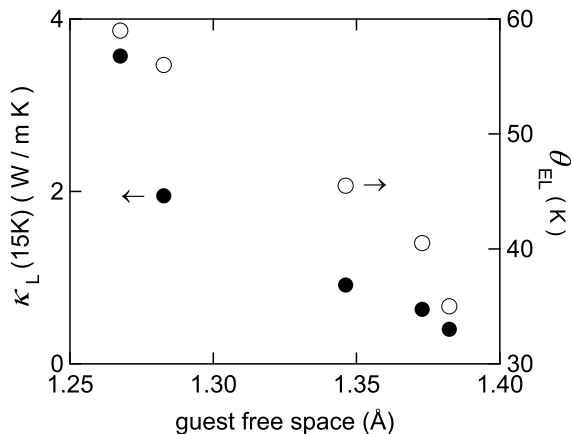


FIG. 7: Dependence of the lower Einstein temperature θ_{EL} and lattice thermal conductivity at 15 K on the guest free space.

space for guest excursion and deforms the restoration potential. We may conclude that this is the main cause of the peak suppression in κ_L , leading to glasslike behavior. Fig. 7 summarizes these results by plotting κ_L at 15 K and θ_{EL} in terms of the guest free space, evaluated semi-quantitatively by subtracting the Sr ionic radius (1.35 Å) and Ga covalent radius (1.26 Å) from the tetrakaidecahedron's radius in each sample.

IV. CONCLUSION

By growing homogeneous single crystals of $\text{Sr}_8\text{Ga}_{16}\text{Si}_{30-x}\text{Ge}_x$ in the full range of $0 \leq x \leq 30$, we were able to gain systematic control of a type-I

clathrate structure's cage size without changing the guest ion or the charge carrier type. The lattice parameter expands by up to 3% with increasing Ge content, and as a consequence the free space for guest excursion increases in the cage. The characteristic energy of the localized $\text{Sr}_{(6d)}$ vibrations decreases from 59 K to 35 K, and the $\text{Sr}_{(6d)}$ behavior clearly evolves from vibrating in an on-center harmonic potential in $\text{Sr}_8\text{Ga}_{16}\text{Si}_{30}$ to a broadened potential in $\text{Sr}_8\text{Ga}_{16}\text{Ge}_{30}$, which allows off-center and anharmonic vibration. This leads to an increase in the effective density of tunneling states and a strong enhancement of the coupling between the $\text{Sr}_{(6d)}$ vibration and the cage acoustic phonons, shortening the latter's mean free path. As a result, the low temperature (1-20 K) lattice thermal conductivity is suppressed in such a way that the crystalline-like peak found for $\text{Sr}_8\text{Ga}_{16}\text{Si}_{30}$ evolves into the well-known glasslike behavior of $\text{Sr}_8\text{Ga}_{16}\text{Ge}_{30}$.

Our results leave little doubt that the described mechanism is the dominant one in producing the anomalous thermal conductivity behaviors observed in these clathrates at low-intermediate temperatures. However, other factors certainly contribute, with variable relevance depending on the particular system or temperature range under study.

Acknowledgments

We thank Y. Shibata for the electron probe microanalysis performed at N-BARD, Hiroshima University. This work was financially supported by the Grants in Aid for Scientific Research (A) (Grant No. 18204032) and the priority area "Skutterudite" (Grant No. 15072205) from MEXT, Japan.

-
- ¹ G. S. Nolas, J. Sharp, and H. J. Goldsmid, *Thermoelectrics - Basic Principles and New Materials Developments* (Springer, New York, 2001).
 - ² B. Eisenmann, H. Schäfer, and R. Zagler, *J. Less-Common Met.* **118**, 43 (1986).
 - ³ K. A. Kovnir and A. V. Shevelkov, *Russian Chem. Rev.* **73**, 923 (2004).
 - ⁴ G. S. Nolas, J. L. Cohn, G. A. Slack, and S. B. Schujman, *Appl. Phys. Lett.* **73**, 178 (1998).
 - ⁵ G. S. Nolas, T. J. R. Weakley, J. L. Cohn, and R. Sharma, *Phys. Rev. B* **61**, 3845 (2000).
 - ⁶ B. C. Sales, B. C. Chakoumakos, R. Jin, J. R. Thompson, and D. Mandrus, *Phys. Rev. B* **63**, 245113 (2001).
 - ⁷ J. L. Cohn, G. S. Nolas, V. Fessatidis, T. H. Metcalf, and G. A. Slack, *Phys. Rev. Lett.* **82**, 779 (1999).
 - ⁸ G. A. Slack, in *CRC Handbook of Thermoelectrics* (Chemical Rubber, Boca Raton, FL, 1995), chap. 34, p. 407.
 - ⁹ G. S. Nolas and C. A. Kendziora, *Phys. Rev. B* **62**, 7157 (2000).
 - ¹⁰ J. Dong, O. F. Sankey, G. K. Ramachandran, and P. F. McMillan, *J. Appl. Phys.* **87**, 7726 (2000).
 - ¹¹ J. Dong, O. F. Sankey, and C. W. Myles, *Phys. Rev. Lett.* **86**, 2361 (2001).
 - ¹² Y. Takasu, T. Hasegawa, N. Ogita, M. Udagawa, M. A. Avila, K. Suekuni, I. Ishii, T. Suzuki, and T. Takabatake, *Phys. Rev. B* **74**, 174303 (2006).
 - ¹³ F. Bridges and L. Downward, *Phys. Rev. B* **70**, 140201(R) (2004).
 - ¹⁴ R. Baumbach, F. Bridges, L. Downward, D. Cao, P. Chesler, and B. Sales, *Phys. Rev. B* **71**, 024202 (2005).
 - ¹⁵ G. K. H. Madsen and G. Santi, *Phys. Rev. B* **72**, 220301(R) (2005).
 - ¹⁶ R. P. Hermann, W. Schweika, O. Leupold, R. Ruffer, G. S. Nolas, F. Grandjean, and G. J. Long, *Phys. Rev. B* **72**, 174301 (2005).
 - ¹⁷ W. Gou, Y. Li, J. Chi, J. H. Ross Jr., M. Beekman, and G. S. Nolas, *Phys. Rev. B* **71**, 174307 (2005).
 - ¹⁸ I. Zerec, V. Keppens, M. A. McGuire, D. Mandrus, B. C. Sales, and P. Thalmeier, *Phys. Rev. Lett.* **92**, 185502 (2004).

- ¹⁹ R. P. Hermann, V. Keppens, P. Bonville, G. S. Nolas, F. Grandjean, G. J. Long, H. M. Christen, B. C. Chakoumakos, B. C. Sales, and D. Mandrus, *Phys. Rev. Lett.* **97**, 017401 (2006).
- ²⁰ A. Bentien, M. Christensen, J. D. Bryan, A. Sanchez, S. Paschen, F. Steglich, G. D. Stucky, and B. B. Iversen, *Phys. Rev. B* **69**, 045107 (2004).
- ²¹ K. Umeo, M. A. Avila, T. Sakata, K. Suekuni, and T. Takabatake, *J. Phys. Soc. Jpn.* **74**, 2145 (2005).
- ²² M. A. Avila, K. Suekuni, K. Umeo, H. Fukuoka, S. Yamanaka, and T. Takabatake, *Phys. Rev. B* **74**, 125109 (2006).
- ²³ M. A. Avila, D. Huo, T. Sakata, K. Suekuni, and T. Takabatake, *J. Phys.: Condens. Matter* **18**, 1585 (2006).
- ²⁴ A. Bentien, S. Johnsen, and B. B. Iversen, *Phys. Rev. B* **73**, 094301 (2006).
- ²⁵ M. A. Avila, K. Suekuni, K. Umeo, and T. Takabatake, *Physica B* **383**, 124125 (2006).
- ²⁶ A. Bentien, V. Pacheco, S. Paschen, Y. Grin, and F. Steglich, *Phys. Rev. B* **71**, 165206 (2005).
- ²⁷ V. Pacheco, A. Bentien, W. Carrillo-Cabrera, S. Paschen, F. Steglich, and Y. Grin, *Phys. Rev. B* **71**, 165205 (2005).
- ²⁸ J. M. Ziman, *Electrons and Phonons* (Oxford University Press, 1960).
- ²⁹ M. Imai, K. Nishida, T. Kimura, and K. Yamada, *J. Alloys. Comp.* **335**, 270 (2002).
- ³⁰ W. Carrilo-Cabrera, R. C. Gil, and Y. Grin, *NCS* **217**, 179 (2002).
- ³¹ N. Nakagawa, M. Miyake, H. Hayase, and T. Koyanagi, *Thermoelectric Conversion Symp. Proc.* (Tokyo, Japan) pp. 136–137 (2002).
- ³² J. Martin, S. Erickson, G. S. Nolas, P. Alboni, T. M. Tritt, and J. Yang., *J. Appl. Phys.* **99**, 044903 (2006).
- ³³ J. E. Graebner, B. Golding, and L. C. Allen, *Phys. Rev. B* **34**, 5696 (1986).